P2.22

ANALYSIS OF PRECIPITATION FORECASTS FROM THE NCEP GLOBAL FORECAST SYSTEM

Huiling Yuan [1,*], Chungu Lu [1,2], Ed Tollerud [1], John McGinley [1], and Paul Schultz [1]
1. NOAA/Earth System Research Laboratory (ESRL)/Global Systems Division (GSD)
2. Cooperative Institute for Research in the Atmosphere (CIRA), Colorado State University

1. INTRODUCTION

Satellite observations extend precipitation measurements from limited-area land surface analyses to a nearly global view of precipitation. As a result, we are able to verify quantitative precipitation forecasts (QPF) from global forecasts. In this study, QPF from the NCEP (National Centers for Environmental Prediction) global forecast system (GFS) have been analyzed with different lead times from 1 to 7 days during the period of October 2005 – September 2006. QPFs over major continents and oceans were composited to verify regional precipitation at various thresholds.

The PERSIANN (Precipitation Estimation from Remotely Sensed Information using Artificial Neural Networks, Sorooshian et al. 2000) precipitation estimates were used as the observations. Using the PERSIANN products, forecast skill [e.g., root mean square error (RMSE) and equitable threat score (ETS)] and other verification metrics for the GFS QPF were compared for different seasons (winter/summer), regions (land/ocean), and zonal districts (tropical, subtropical, and midlatitudes). Daily QPF for the year demonstrated widely varying forecast skill over different subregions. Since upstream weather over the Pacific Ocean is critical for predicting weather over the continental United States (CONUS), it is important to know both the predictability of QPF and what forecast skill precipitation forecasts process over the ocean.

Ebert et al. (2007) compared different near-real-time satellite precipitation estimates and used the satellite data to verify short-range precipitation forecasts from mesoscale models over several continents. As an alternative observation data, the NCEP CMORPH (CPC MORPHing technique, Joyce et al.2004) satellite precipitation estimates will be used to study the GFS QPF in the future. Uncertainties in the observations are also needed to be considered, since uncertainties in observation data greatly affect forecast skill in verification.

We discuss application of this study to future research for projects related to THORPEX (The Observing-System Research and Predictability Experiment), a long-term research program organized under the World Meteorological Organization's World Weather Research Program, and the next-generation global models, such as Finite-volume Icosahedral Model (FIM) at NOAA/ESRL/GSD.

2. DATA

Currently, the NOAA/ESRL/GSD data repository routinely archives the NCEP operational GFS forecasts. Since June 2005, the GFS runs to 180 hours (7.5 days) at T382L64 (~ 40 km) resolution, and then at T190L64 (~ 70 km) to 384 h, four times per day (06, 12, 18, 24 UTC). The data is archived on 1 x 1 degree to 180 hours. The PERSIANN 0.25 x 0.25 degree satellite-derived precipitation estimates provided by University of California, Irvine were selected to verify the 1 x 1 degree global QPF. The PERSIANN data covers nearly global (50°S-50°N) domain with 6-h interval. The data is available since March 2000.

The 24-h precipitation accumulations of the PERSIANN data were aggregated to the 1 x 1 degree GFS grid pixels to verify the GFS QPF with different lead times on the concomitant PERSIANN 1x1 degree grid pixels. The results presented in this paper are from the 1200 UTC forecast cycle.

3. METHOD

Many verification metrics are introduced in two verification books (Wilks 2006, Jolliffe and Stephenson 2003). The RMSE value is a straightforward comparison to measure forecast

* Corresponding author address: Huiling Yuan, NOAA/ESRL, R/GSD7, 325 Broadway, Boulder, CO, 80305-3328. email: huiling.yuan@noaa.gov

errors between the observations and corresponding forecasts. The ETS, a common score used in current operational weather forecasting systems, is defined as:

$$ETS = \frac{a - a_r}{a - a_r + b + c} \qquad (3.1),$$

where *a* is the number of hit events (forecasted the events that were observed), *b* is the number of false alarm events, *c* is the missing events, *d* is the number of corrected rejection, and *n* is the total number of events ($n = a + b + c + d$); and a_r is the number of hits for random forecasts, given by:

$$a_r = \frac{(a+b)(a+c)}{n} \qquad (3.2).$$

The ETS ranges from -1/3 to 1 with the best value of 1 and skillful values of being positive.

Six thresholds 0.01, 0.1, 0.25, 0.5, 1, and 2 inches/24-h (i.e., 0.254, 2.54, 6.35, 12.7, 25.4, 50.8 mm/24-h) were selected to calculate the ETS for each grid pixel during a season. The cool season is from October 2005 to March 2006 (winter in the Northern Hemisphere), while the warm season is from April to September 2006 (summer in the Northern Hemisphere). The ETS was also computed for a selected region for all available observed and forecasted grid pixels. The subregions can be different continents and oceans, or zonal regions.

4. RESULTS

Figure 1 shows the spatial distribution of average 24-h precipitation accumulations on available PERSIANN and corresponding GFS QPF grids during the cool season. General precipitation bands in PERSIAAN are along the ITCZ (intertropical convergence zone), South America, South Africa, and the western Pacific Ocean. The GFS QPF follows a similar pattern for the lead times of 1, 4, and 7 days, but with wet biases over these precipitation bands and larger biases over the oceans. The warm season (not shown) shows similar precipitation bands along the equatorial areas and stronger precipitation over the lands of the Northern Hemisphere.

The RMSE during a season is shown in Fig. 2. The errors are larger in the observed heavy precipitation areas. With the increasing forecast lead time, the RMSE increases and the errors propagate eastward. The forecast errors of the QPF are large over the oceans and the Southern Hemisphere during the cool season, while the RMSE enlarges over the continents of the Northern Hemisphere during the warm season.

The ETS is computed on each grid pixel (Fig. 3.) for six selected thresholds. The shaded area represents grids having occurred events. With a 1-day lead time, the QPF shows good skill from 0.01 inches (0.254 mm) to 0.5 inches (12.7 mm) and limited skill for higher thresholds. Forecast skill greatly reduces with the increasing lead time (not shown). The ETS is associated with precipitation thresholds and is not independent with the biases. During the warm season (not shown), the ETS shows more skillful forecasts over the continents of the Northern Hemisphere and less skill over the oceans compared to the cool season.

The total 11 zones (Fig. 4) are defined based on the locations of the continents and oceans. The geographical regions are not completely independent. The upstream weather over the North Pacific Ocean (the NP region) is associated with the weather over the North America (the NAm region). The RMSE for one year (Fig. 5) shows stronger seasonal variations over the continental zones (Figs. 5a, 5b, 5c) than over the oceanic zones (Figs. 5d, 5e). The Northern and Southern Hemispheres show reverse trends over the continents due to the season switch, but there are no obvious season signals over the oceans due to smaller climate variability.

Similarly, the ETS is computed for each zone (Fig. 6) during the cool and warm seasons, respectively. The oceanic zones have more samples than the continental zones and show similar values for each oceanic zone with less seasonal variability. QPFs over the continents of the Southern Hemisphere continents (SAf, Au, SAm) present better forecast skill than those over the Northern Hemisphere continents (NAf, Asi, NAm), especially for smaller thresholds and during the cool season. With the increasing forecast lead time, forecast skill reduces and the QPF becomes unskillful at higher thresholds. With a 1-day lead time, the oceans tend to have better skill at higher thresholds than the continents. This is consistent with the spatial distribution of the ETS (Fig. 3).

Also, the seven zonal regions, including one equatorial region (10°S-10°N), two tropical regions (10°N-25°N, 10°S-35°S), two subtropical regions (25°N-35°N, 25°S-35°S), and two midlatitude regions (35°N-49°N, 35°S-49°S), are used to compare forecast skill for corresponding observations and forecasts over each region during a season (not shown). Generally, the equatorial zone shows higher skill, while the southern midlatitude zone (35°S-49°S) shows lower skill. During the cool season, the southern subtropical and tropical zones are better than the northern latitudinal zones with the lead times of 1 to 5 days. During the warm season, forecast skill over the northern zonal zones increases, while both northern and southern subtropical zones have better skill than other zonal zones with the lead times of 1 to 5 days. With a 7-day lead time, the equatorial zone has better skill.

5. SUMMARY

By means of satellite precipitation estimates, a nearly global view of forecast skill for the GFS is feasible. Forecast skill of the GFS QPF for one-year assessments shows large variations in terms of the GFS performance for different continents and oceans, seasons, and lead times. More GFS data from other years are needed to study the trend of forecast skill over different regions.

On the other hand, the quality of satellite estimates highly impacts the verification results of the forecasts. Cross-validation needs to be conducted for evaluating different satellite data, especially over the oceans. Further verification schemes should track the propagation of a high-impact weather system from the upstream ocean to the downstream continent. For example, the preceding severe storms over the North Pacific Ocean are areas of interest to forecast the weather over the North America.

The preliminary results indicate that forecast skill of the global QPF needs to be investigated thoroughly, such as the intercomparison of the GFS and high-resolution mesoscale models over the land and ocean. The differences of forecast skill over different regions are associated with precipitation thresholds and regional weather systems. In addition, the physics of the GFS is uniform for all locations at the model resolution (~ 40 km). As the satellite estimates are available, a higher-resolution GFS or higher resolution of the GFS output is needed to study predictability of QPF for different systems.

The study can be extended to verify other global models (e.g., the NOAA FIM model) and other variables (e.g., winds and moisture). Ensemble forecasting provides a promising tool for weather forecasts. Verification of the QPF and other important variables on a probabilistic sense, such as probabilistic QPF (PQPF), is a key component for the THORPEX TIGGE (THORPEX Interactive Grand Global Ensemble) project.

6. ACKNOWLEDGEMENTS

This research was performed while the first author held a National Research Council Research Associateship Award at NOAA/ESRL.

7. REFERENCES

Ebert, E. E., J. E. Janowiak, and C. Kidd, 2007: Comparison of near-real-time precipitation estimates from satellite observations and numerical models. *Bull. Amer. Meteor. Soc.*, **88**, 47–64.

Jolliffe, I. T., and D. B. Stephenson, 2003: *Forecast Verification. A Practitioner's Guide in Atmospheric Science*. Wiley and Sons Ltd.

Joyce, R. J., J. E. Janowiak, P. A. Arkin, and P. Xie, 2004: CMORPH: A method that produces global precipitation estimates from passive microwave and infrared data at high spatial and temporal resolution. *J. Hydrometeor.,* **5,** 487–503.

Sorooshian, S., K.-L. Hsu, X. Gao, H. V. Gupta, B. Imam, and D. Braithwaite, 2000: Evaluation of PERSIANN system satellite-based estimates of tropical rainfall. *Bull. Amer. Meteor. Soc.,* **81,** 2035–2046.

Wilks, D. S., 2006: *Statistical Methods in the Atmospheric Sciences.* 2d ed. Elsevier Academic Press, 627 pp.

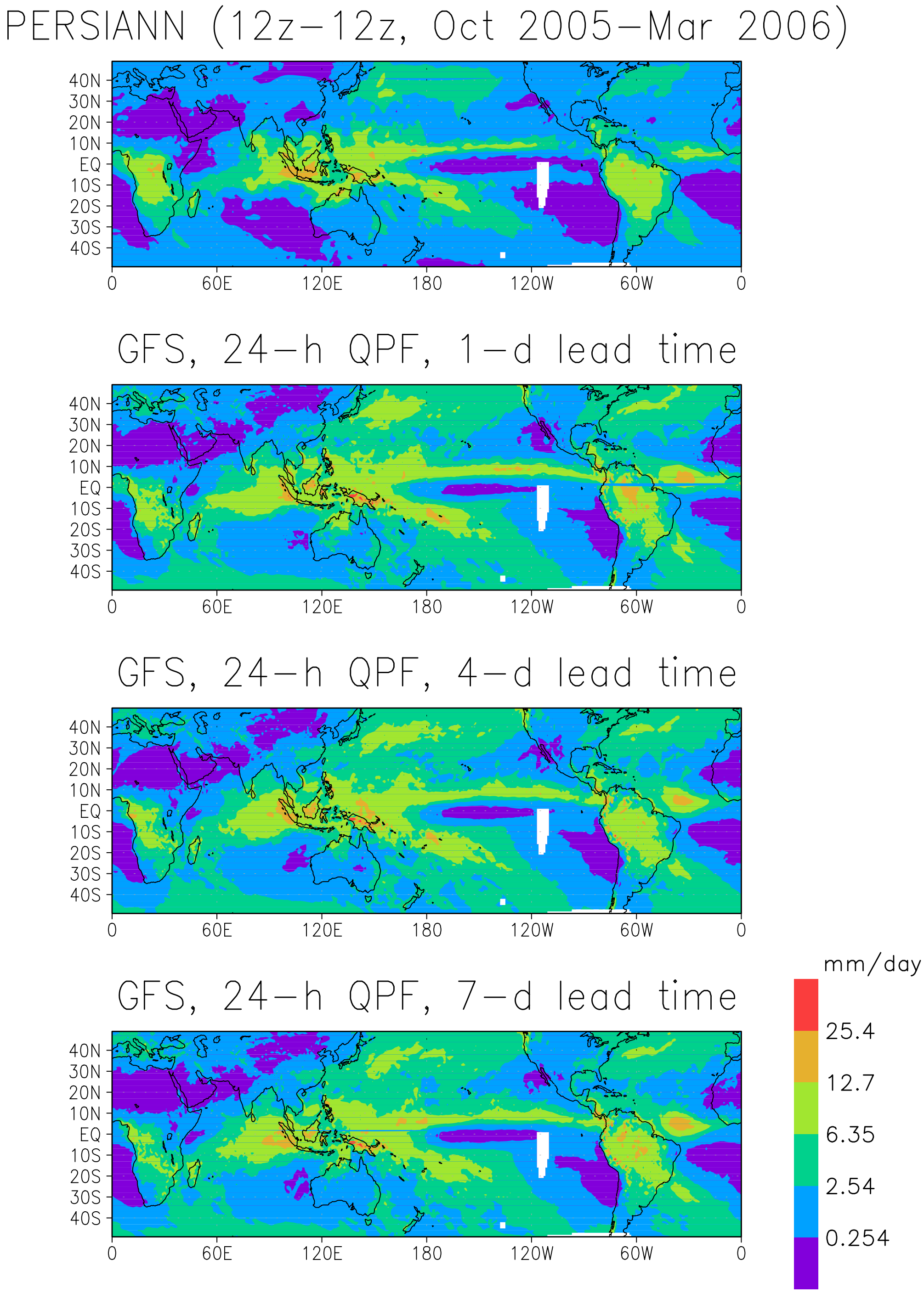

Fig. 1. Average 24-h precipitation accumulations during October 2005-March 2006 for PERSIANN (top panel) data and the GFS QPF with lead times of 1, 4, and 7 days (bottom three panels). The blank area has no data from PERSIANN during the period.

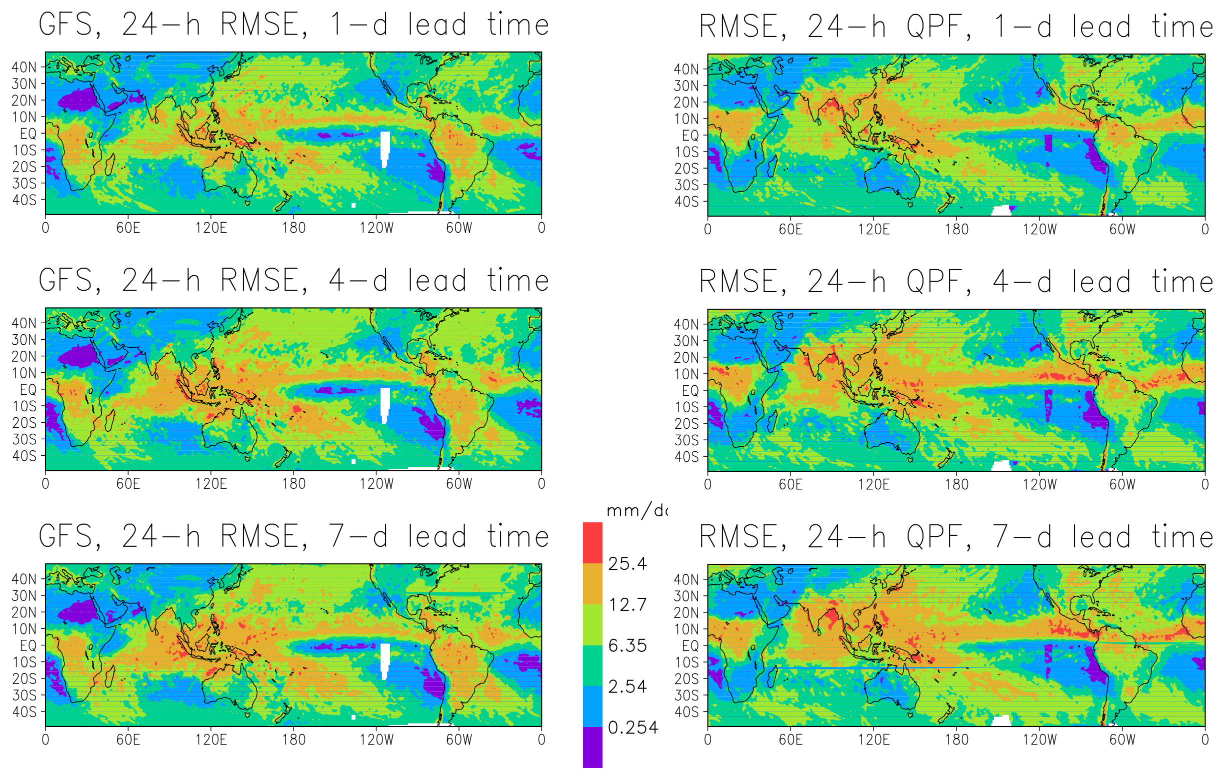

Fig. 2. The RMSE for 24-h QPF with the lead times of 1, 4, 7 days during October 2005-March 2006 (left column) and during April-September 2006 (right column). Blank areas have no PERSIANN data.

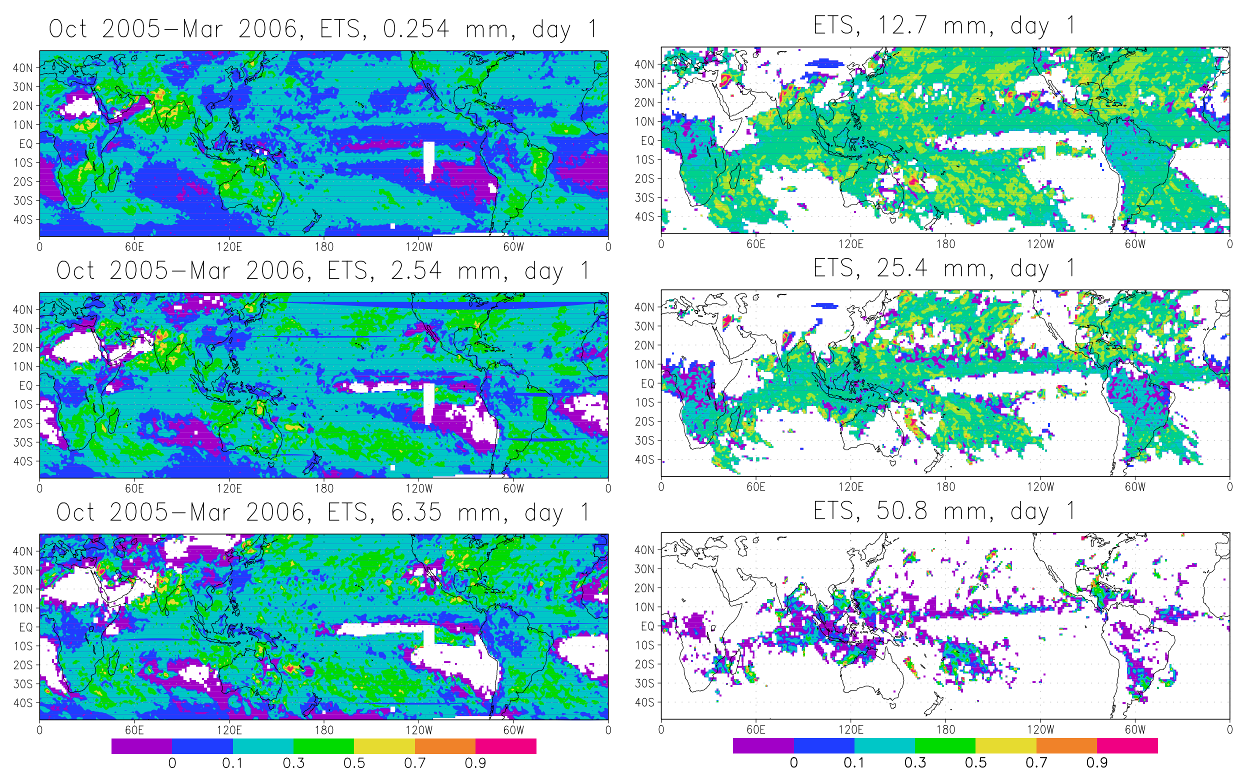

Fig. 3. The ETS for 24-h QPF with a 1-day lead time during October 2005-March 2006. Six thresholds are shown in the titles. Blank areas indicate no events at the selected threshold during the period.

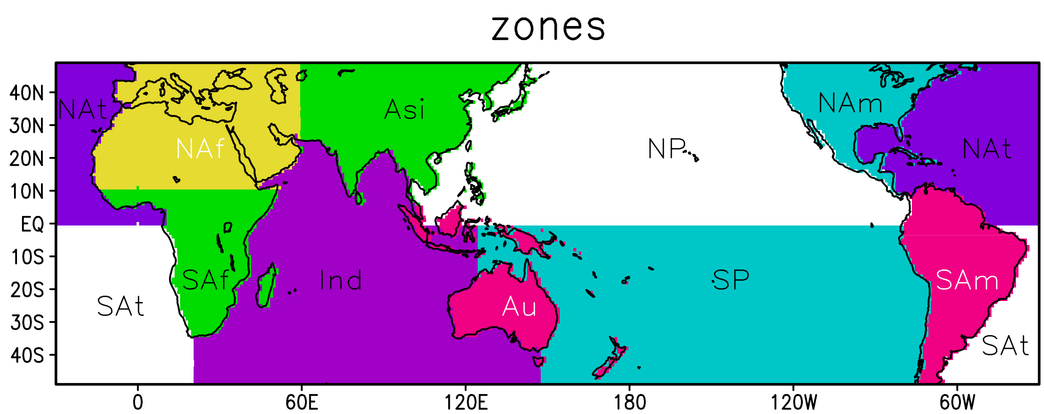

Fig. 4. The 11 zones dividing the continents and oceans. NAf: North Africa and West Asia, SAf: South Africa, Asi: Asia, Au: Australia, NAm: North America, SAm: South America, NAt: North Atlantic Ocean; SAt: South Atlantic Ocean, Ind: Indian Ocean, NP: North Pacific Ocean, and SP: South Pacific Ocean.

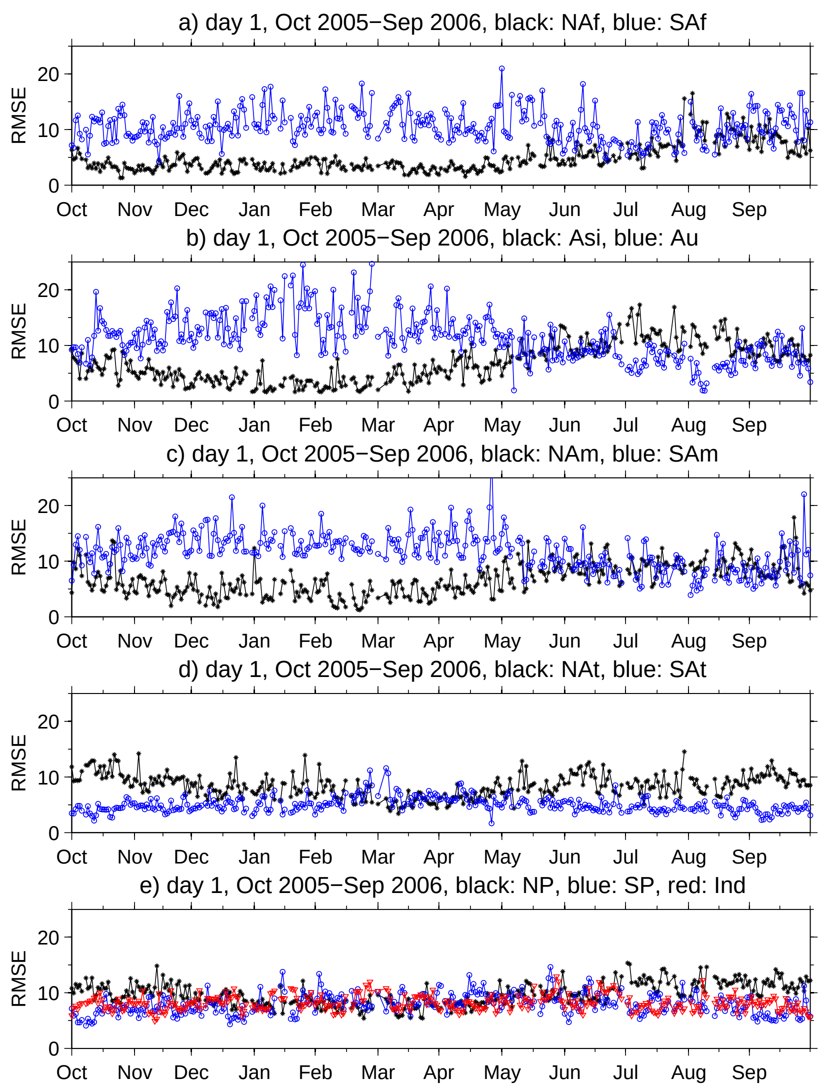

Fig. 5. The RMSE of 24-h QPF with a 1-day lead time over the 11 zones during October 2005-September 2006. NAf and SAf (a), Asi and Au (b), Nam and Sam (c), Nat and Sat (d), and NP, SP, and Ind (e).

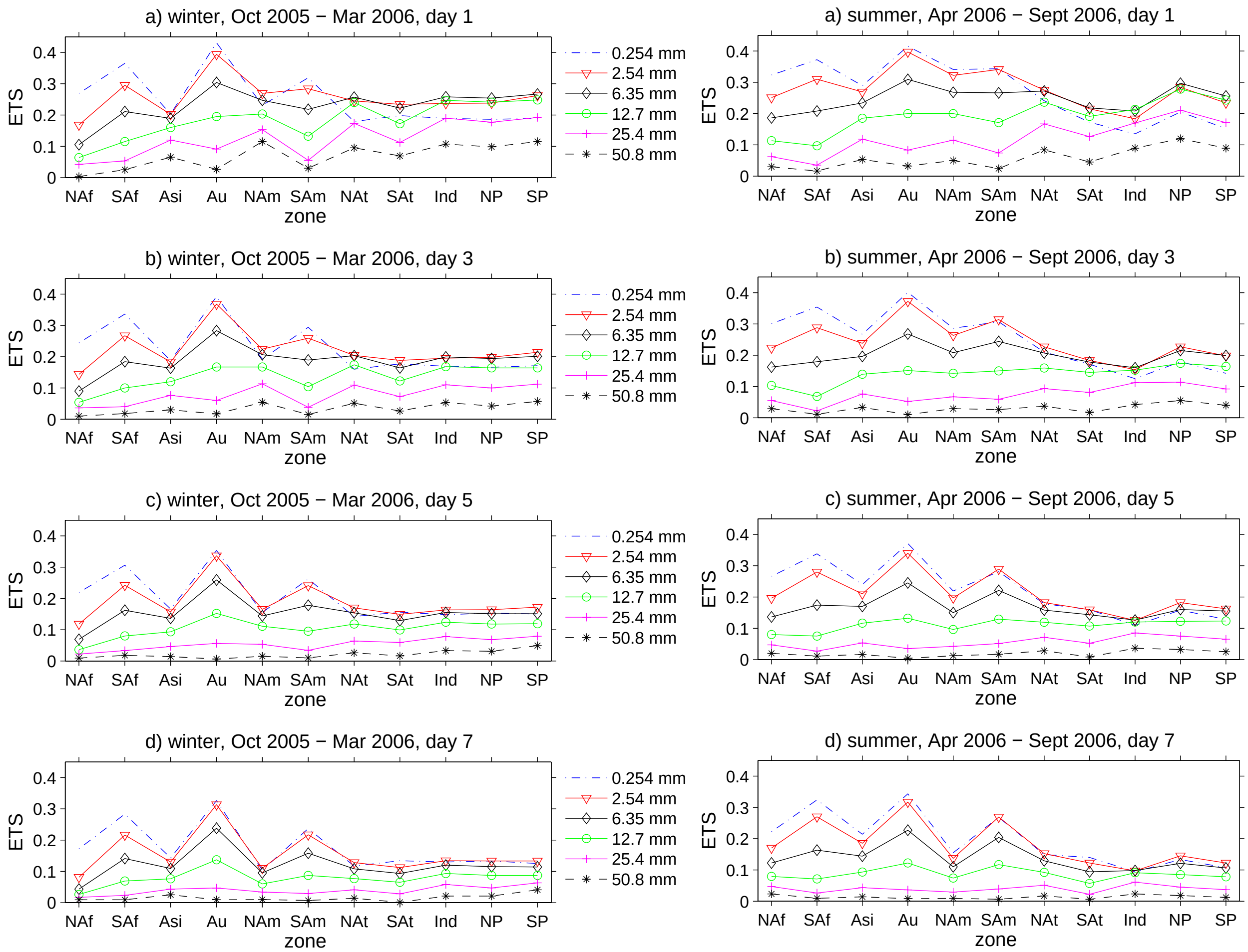

Fig. 6. The ETS for 24-h QPF with the lead times of 1, 3, 5, 7 days (a, b, c, d) over the 11 zones during October 2005-March 2006 (left column) and during April-September 2006 (right column). Six thresholds are shown in the labels.